Journal of Hazardous Materials 382 (2020) 121018

Contents lists available at ScienceDirect

Journal of Hazardous Materials

journal homepage: www.elsevier.com/locate/jhazmat

Broad spectrum detection of veterinary drugs with a highly stable metal-organic framework

Bin Wang[a], Jing-Hao Liu[b], Jiamei Yu[b,*], Jie Lv[a], Chen Dong[a], Jian-Rong Li[a,*]

[a] Beijing Key Laboratory for Green Catalysis and Separation, College of Environmental and Energy Engineering, Beijing University of Technology, Beijing 100124, PR China
[b] College of Materials Science and Engineering, Beijing University of Technology, Beijing 100124, PR China

GRAPHICAL ABSTRACT

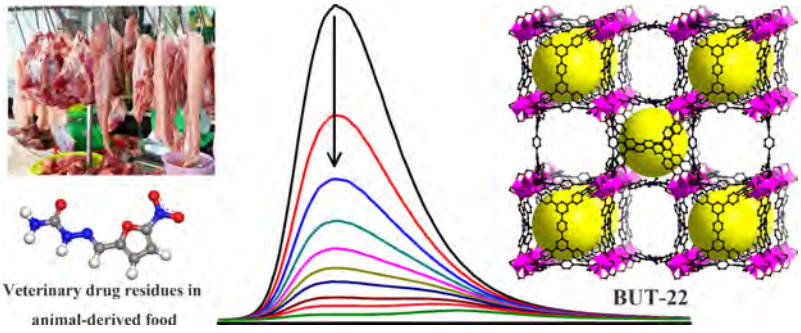

ARTICLE INFO

Editor: G. Li Puma

Keywords:
Broad spectrum detection
Fluorescence quenching
Metal-organic frameworks (MOFs)
Veterinary drugs

ABSTRACT

The broad spectrum detection of veterinary drugs is very important for rapid and large-scale safe screen of animal-derived foods. Metal-organic frameworks (MOFs), as a kind of emerged functional porous materials are quite promising in the chemical sensing and molecular detection. In this work, we report the high-performance broad spectrum detection of 15 commonly-used veterinary drugs through the fluorescence quenching in a newly-designed chemically stable Al-based MOF, $Al_3(\mu_3\text{-}O)(OH)(H_2O)_2(PPTTA)_{3/2}$ (BUT-22). To the best of our knowledge, this is the first systematic investigation for the application of MOFs in the detection/sensing of veterinary drugs through fluorescence quenching method. The quenching efficiencies of the tested veterinary drugs on BUT-22 are all beyond 82%, and the limits of detection (LOD) are low at parts per billion (ppb) levels. Interestingly, BUT-22 also enables the selective detection of nicarbazin (NIC) through the clearly-observed red shift of its maximum fluorescence emission wavelength. Moreover, the fluorescence quenching mechanism was explored with the help of theoretical calculations. Our work indicates that MOFs are favorable materials for the detection of veterinary drugs, being potentially useful in monitoring drug residues of animal-derived foods.

1. Introduction

Veterinary drugs are frequently used in animals to combat infections and induce growth. However, these drugs can be accumulated in animal tissues and the residues can cause severe risks to human health, such as toxic effects and allergic reactions. Another consequence is the development of resistant bacteria, which might interfere in the efficiency of veterinary drugs and even difficult diseases treatment (Ritter et al., 2006). In order to increase food safety, maximum residue levels (MRLs) are established for veterinary drugs in different kinds of food

* Corresponding author.
E-mail addresses: jyu@bjut.edu.cn (J. Yu), jrli@bjut.edu.cn (J.-R. Li).

https://doi.org/10.1016/j.jhazmat.2019.121018
Received 12 January 2019; Received in revised form 6 July 2019; Accepted 13 August 2019
Available online 14 August 2019
0304-3894/

(Passantino and Russo, 2008). Therefore, the development of sensitive analytical methodologies for the detection of these compounds is of paramount interest. The detection of veterinary drug residues in foodstuff samples was typically performed based on instrumental methods such as by gas chromatography (GC) coupled to electron capture detection (ECD) (Iglesias-Garcia et al., 2008; Aulakh et al., 2006), mass spectrometry (MS) (Fernandez-Alvarez et al., 2009; Guo et al., 2009) or tandem mass spectrometry (MS/MS) (Carro et al., 2005). These instrumental methods, however, share some common drawbacks, such as high cost, complex sample preparation process, time-consuming, and require complex equipment and trained personnel. In addition, instrumental methods are also disadvantageous in the rapid and large-scale screening of animal-derived food samples and the self-examination of livestock farms. Therefore, the development of a simple and broad spectrum veterinary drug detection method is highly desired.

Optical sensing by utilizing the change in fluorescence readout induced by sensor-analyte interactions is a powerful detection method (You et al., 2015). Metal-organic frameworks (MOFs) built by metal ions/clusters and organic linkers are a class of emerging functional porous materials. The superior properties of high specific surface areas, tunable composition and structure, and facile functionalization endow them with many advantages compared to the traditional materials in applications of chemical detection (Kreno et al., 2012; Lustig et al., 2017; Wang et al., 2018; Zhu et al., 2018), molecule reorganization (Sawano et al., 2015; Zhang et al., 2015), gas storage (Li et al., 2014; Spanopoulos et al., 2016), separation (Nugent et al., 2013; Cui et al., 2016; Liao et al., 2017; Hu et al., 2018), catalysis (Jiang et al., 2014; Yang et al., 2018; Zhang et al., 2018; Tang and Wang, 2018; Zhang et al., 2017a; Deria et al., 2016), proton conduction (Joarder et al., 2017), and so on. Particularly, large numbers of MOFs possess unique optical properties. This type of MOFs, also known as luminescent MOFs (LMOFs) are promising candidates for sensing applications (Kreno et al., 2012; Lustig et al., 2017; Liu et al., 2017; N'Dala-Louika et al., 2017). In previous work, we reported the design and synthesis of two highly stable Zr-MOFs, BUT-12 and -13 for the selective detection of antibiotics (Wang et al., 2016). The detection limits of the two MOFs toward the several antibiotic molecules are ppb levels, showing MOFs are promising in the drugs detection. However, it was confirmed that the fluorescence of most Zr-MOFs is ligand centered, and their change is mainly based on the interactions between the analytes and the organic ligands in MOFs (Bai et al., 2016). For some veterinary drug molecules, the interactions of them with organic ligands in Zr-MOFs are too weak to cause the fluorescence change. In addition, in the actual animal-derived foods, various of veterinary drugs are often co-exist. Broad spectrum detection of their residues is thus very important. Therefore, new MOFs should be developed for the broad spectrum detection of veterinary drugs. In addition to Zr-MOFs, Al-based MOFs also possess good chemical stability such as in water and prominent fluorescent properties (Yang et al., 2013). Besides the organic ligands, the Al metal centers can also provide fluorescence, which can provide additional interaction sites for drug molecules. Typically, large number of Al-MOFs are constructed from the classical $Al_3(\mu_3\text{-}O)(OH)(H_2O)_2(COO)_6$ secondary building unit (SBU), which contains the terminal coordinated H_2O/OH groups. In addition, most veterinary drug molecules contain $-OH$ or $-NH_2$ group, which can form hydrogen bonding interactions with the terminal coordinated H_2O/OH groups mentioned above, thus leading to the sensitive fluorescence change of Al-MOFs, thereby achieving high-performance broad spectrum detection of the veterinary drugs.

In this work, a new chemically stable Al-MOF, $Al_3(\mu_3\text{-}O)(OH)(H_2O)_2(PPTTA)_{3/2}$ (BUT-22, $PPTTA^{4-}$ = 4,4′,4″,4‴-(1,4-phenylenebis(pyridine-4,2,6-triyl))tetrabenzate, BUT = Beijing University of Technology) with a *soc*-a topological framework structure was designed and synthesized for the broad spectrum detection of veterinary drugs. BUT-22 shows excellent chemical stability, high surface area, moderate pore sizes, and good fluorescent emission. Fifteen veterinary drugs of six classes: nitrofurans (NFs), sulfonamides (SAs), tetracyclines, chloramphenicols (CPs), anticoccidial drugs, and anthelmintic drugs were then studied. It was found that the quenching efficiencies of the selected 15 veterinary drugs on BUT-22 all beyond 82% and the limits of detection (LOD) of BUT-22 toward these veterinary drugs are low at ppb levels. More interestingly, this MOF also enables the selective detection of nicarbazin (NIC).

2. Materials and methods

2.1. Synthesis

All general reagents and solvents (AR grade) were commercially available and used as received. The ligand acids, H_4PPTTA and H_4BCQDA were synthesized according to our previous work (Wang et al., 2017). Al-soc-MOF-1 was synthesized according to the literature method (Alezi et al., 2015).

$[Al_3(\mu_3\text{-}O)(OH)(H_2O)_2(PPTTA)_{3/2}]\cdot S$ (BUT-22·S) (S represents non-assignable solvent molecules). $Al(NO_3)_3{\cdot}9H_2O$ (100 mg, 0.26 mmol), H_4PPTTA (50 mg, 0.07 mmol), and propionic acid (3.0 mL) were ultrasonically dissolved in 15 mL of DMF in a 20 mL Teflon-lined stainless-steel autoclave. The autoclave was then heated at 150 °C for 48 h in an oven. After cooling to room temperature (RT) spontaneously, the resulting colorless crystals were harvested by filtration and washed with DMF and acetone, and then dried in air (yield 73 mg). FT-IR (KBr pellets, cm^{-1}): 3392 (w), 1646(s), 1589(s), 1533(m), 1381(s), 1243(w), 1098(w), 1003(w), 795(m).

2.2. Single-crystal X-ray diffraction

The crystal data of BUT-22 were collected on a Rigaku MicroMax-007HF diffractometer equipped with a graphite-monochromatic enhanced Cu Kα radiation (λ = 1.54184 Å) at 100 K. The datasets were corrected by empirical absorption correction using spherical harmonics, implemented in the *SCALE3 ABSPACk* scaling algorithm. The structure of BUT-22 was solved by direct methods and refined by full-matrix least-squares on F^2 with anisotropic displacement using the *SHELXTL* software package. Non-hydrogen atoms were refined with anisotropic displacement parameters during the final cycles. Hydrogen atoms of the ligands were calculated in ideal positions with isotropic displacement parameters. Those in OH groups and coordinated H_2O molecules were not added but were calculated into molecular formula of the crystal data. There are large solvent accessible pore volumes in the crystals of BUT-22, which are occupied by highly disordered solvent molecules. No satisfactory disorder model for these solvent molecules could be assigned, and therefore the *SQUEEZE* program implemented in *PLATON* was used to remove the electron densities of these disordered species (Spek, 2003). Thus, all of electron densities from free solvent molecules have been "squeezed" out. The details of structural refinement can be found in Tables S1 and the cif file.

2.3. Activation of the as-synthesized MOF sample

As-synthesized sample of BUT-22 or Al-soc-MOF-1 sample was firstly soaked in fresh DMF for 24 h and then the extract was discarded. Fresh acetone was subsequently added, and the sample was allowed to stay in it for 4 h. This procedure was repeated three times over one day. After decanting the acetone extract, the sample was dried under a dynamic vacuum ($< 10^{-3}$ Torr) at RT for 3 h. Before adsorption measurement, the sample was further activated using the "outgas" function of the adsorption analyzer at 90 °C for 10 h.

2.4. Fluorescence measurements

The finely grounded powder sample of BUT-22 or Al-soc-MOF-1 (5 mg) was immersed in 40 mL of DMF and ultrasonicated for 30 min to form stable turbid suspension (Fig. S10), then 1 mL of it was added to a cuvette. The fluorescence upon excitation at 280 nm of BUT-22 (or 285 nm of Al-soc-MOF-1) was measured in-situ after incremental

addition of freshly prepared analyte solution (0.3 μM). The mixed solution was stirred at constant rate during experiment to maintain its homogeneity. All the experiments were performed in triplicate, and consistent results are reported.

2.5. Aqueous-phase adsorption

Freshly prepared BUT-22 sample (10 mg) was totally activated and then transferred into DMF solutions of nitrofurazone (NZF) and tetracycline (TCY) with given concentrations (10 ppm) in a vial, respectively. UV − vis spectra of the solutions were recorded to characterize the adsorption performances of BUT-22 along with the soaking time at 298 K.

2.6. Calculation details

The possible binding sites of NIC in BUT-22 were calculated by conventional grand canonical monte carlo (GCMC), using Sorption program in Materials Studio software. The simulation boxes contain $1 \times 1 \times 1$ unit cells. The Metropolis method was used in all simulation process. The long-range electrostatic interactions were dealt with the Ewald summation technique. The vdW interactions were described by a 12-6 Lennard-Jones (LJ) potential using parameters from the universal force field (UFF) (Rappe et al., 1993) and a cutoff radius of 14 Å. The charges of BUT-22 were calculated using the charge equilibration (Q_{eq}) method as implemented in Material Studio. The charges and geometry optimization of NIC were calculated using the DFT method. The DFT calculations are performed with the Dmol3 program in Material Studio software. The Perdew-Burke-Ernzerhof (PBE) method based on the generalized gradient approximation (GGA) was used.

2.7. Cyclic tests

In a typical experimental setup, 5 mg finely grounded sample of BUT-22 or Al-soc-MOF-1 was weighed and added to a cuvette containing 1.0 mL of DMF under stirring. The fluorescence upon excitation at 280 nm of BUT-22 (or 285 nm of Al-soc-MOF-1) suspension was measured in situ after addition of 500 μL freshly prepared NZF solution (0.3 mM). After measurement, the MOF sample was centrifuged and washed with acetone several times and dried in an 80 °C oven for 1 h to remove the residual solvents. The regenerated sample was used again for the detection of NZF.

3. Results and discussion

3.1. Synthesis and Structure

Solvothermal reaction of H_4PPTTA with $Al(NO_3)_3{\cdot}9H_2O$ in the presence of propionic acid as competing reagent in *N,N'*-dimethylformamide (DMF) yielded cubic-shaped single crystals of $Al_3(\mu_3\text{-}O)(OH)(H_2O)_2(PPTTA)_{3/2}$ (BUT-22). Its' phase purity was checked by PXRD measurement. As shown in Fig. 2a, the experimental PXRD patterns match well with that simulated from the single-crystal data, indicating its' pure phase. In addition, the absence of characteristic bonds near 1696 cm^{-1} for carboxyl groups of free carboxylic acid ligands in the FT-IR spectrum of BUT-22 indicates that the acid ligands are deprotonated, and their carboxylate groups were all coordinated with the metal ions in the MOF (Fig. S1). The TGA curves of BUT-22 are shown in Fig. S2, indicating that it is stable up to *ca.* 470 °C.

Single-crystal X-ray diffraction reveals that BUT-22 crystallizes in cubic *Pm*-3*n* space group. Its framework consists of classical trinuclear $Al_3(\mu_3\text{-}O)$ cluster core (Fig. 1a) linked by elongated tetratopic ligand, $PPTTA^{4-}$ (Fig. 1b). In BUT-22, there exists one crystallographically independent Al atom, which is eight-coordinated in an octahedral coordination geometry (Fig. 1a). Each Al atom is coordinated by four O atoms from different carboxylate groups, one μ_3-O atom, and one terminal − OH/H_2O entities. Three Al atoms connected with each other by one μ_3-O, two H_2O, one −OH, and six carboxyl groups from six different ligands to form a $Al_3(\mu_3\text{-}O)(OH)(H_2O)_2(COO)_6$ secondary building unit (SBU) (Fig. 1a). Furthermore, these SBUs are linked by $PPTTA^{4-}$ ligands to form a 3D framework with embedded cubic cages that are interconnected through square channels along the *a*, *b*, and *c* directions. The edge length of the cubic cage is 15 Å (atom to atom distance). There are two types of interconnected channels in BUT-22, type I is square shaped and type II is almost circular shaped (Fig. 1d) and the edge length of them are all 15 Å (atom to atom distance). From the topological view point, $PPTTA^{4-}$ ligands can be seen as 4-connected nodes and Al_3 clusters serve as 6-connected nodes (Fig. 1a, b), the 3D framework structure of BUT-22 can thus be simplified as a 4,6-coordinated bi-nodal net with the point symbol of $\{4^4{\cdot}6^2\}_3\{4^6{\cdot}8^9\}_2$, which corresponds to the *soc*-a topology according to *Topos* 40 software (Fig. 1e). The total solvent-accessible volume in the framework of BUT-22 was estimated to be 80.5% of its unit-cell volume, as estimated by *PLATON* (Spek, 2003). It should also be pointed out that BUT-22 is iso-structural to a previously reported Al-MOF, Al-soc-MOF-1 constructed from a similar ligand, 5′,5″″-(1,4-phenylene)bis (([1,1':3',1″-terphenyl]-4,4″-dicarboxylate)) ($BCQDA^{4-}$) (Fig. S7a) (Alezi et al., 2015). The difference of between the two ligands is that ring2 in $BCQDA^{4-}$ is a benzene ring and that in $PPTTA^{4-}$ is a pyridine ring (Fig. S7). The absence of H atom on the pyridine N atoms leads to a smaller steric hindrance, thus the dihedral angles between the ring 2 and terminal benzene ring (ring 1) of $PPTTA^{4-}$ (30.3°) is smaller than that (33.8°) in $BCQDA^{4-}$. BUT-22 and Al-soc-MOF-1 thus provide a good platform for exploring the effect of the functional groups in ligands on the sensing performances of MOFs as discussed below.

3.2. Porosity and stability

The permanent porosity of BUT-22 has been confirmed by N_2 sorption at 77 K and PXRD measurements (Fig. 2). Saturated N_2 uptake of 1371 cm^3 (STP) g^{-1} was achieved, and the evaluated BET surface area is 4488 $m^2\,g^{-1}$. The experimental total pore volume for BUT-22 is 2.11 $cm^3\,g^{-1}$, being in close to the calculated value of 2.12 $cm^3\,g^{-1}$ based on *PLATON* calculation (Spek, 2003). Based on the N_2 adsorption data, the pore size distributions were calculated by density functional theory (DFT) method, which gave two types of pores of 19 and 22 Å for BUT-22 (Fig. 2b, insert). In addition, we also measured the N_2 sorption isotherm of Al-soc-MOF-1 at 77 K (Fig. S4). Saturated N_2 uptake of 1501 cm^3 (STP) g^{-1} was achieved, and the evaluated BET surface area is 4089 $m^2\,g^{-1}$. In order to examine the chemical stabilities of BUT-22, its sample was treated in water and pH = 1 HCl aqueous solution at RT. After being soaked in these solutions for 24 h, the measured PXRD patterns show retained crystallinity and unchanged structure (Fig. 2a). Furthermore, the N_2 sorption isotherms for the samples after being treated in the solutions mentioned above were measured and almost the same uptakes were observed as that of the pristine sample, which further confirms the framework stability of BUT-22 under these conditions (Fig. 2b).

3.3. Detection of veterinary drugs

The solid-state fluorescent properties of BUT-22 as well as its' ligand acid were firstly measured at RT. Experimentally, finely grounded powder samples of BUT-22 were immersed in DMF solution and then ultrasonicated over 30 min to form a steady turbid suspension. Interestingly, we found that the suspension was stable in a short time period of operation. Even after 6 h there is almost no precipitate found in the bottom of the bottle (Fig. S10a). In addition, we also checked the fluorescence of the blank BUT-22 solution at different times. We found that, even after 4 h, the fluorescence of BUT-22 solution was almost the same with the as-prepared one, further confirming the stability of the MOF solution (Fig. S10b). In order to check the consistency of the particle size, SEM of the suspension was measured, and we found the particle size of BUT-22 solution is about 200 nm (Fig. S10c), being basically uniform and quite small. The small and uniform particles are indeed

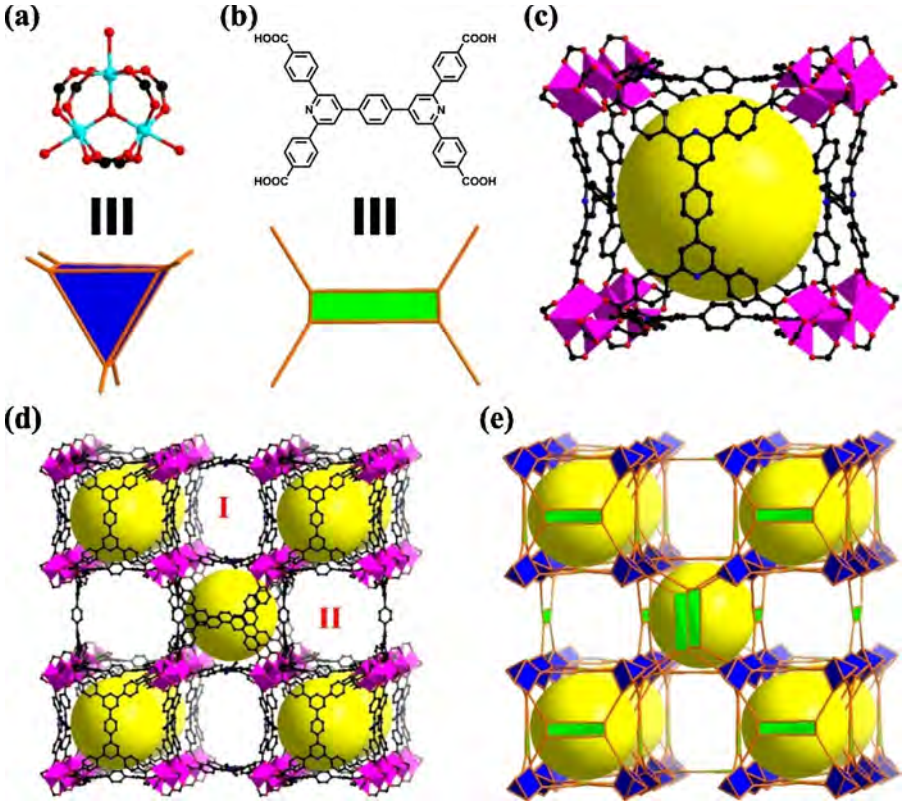

Fig. 1. Construction and the structure of BUT-22: (a) $Al_3(\mu_3\text{-}O)(OH)(H_2O)_2(COO)_6$ SBU and simplified 6-connected node, (b) H_4PPTTA ligand acid and simplified 4-connected node; (c) the cubic cage in BUT-22; (d) framework structure of BUT-22 (H atoms are omitted for clarity. color code: Al, wathet-blue; C, black; O, red; and N, blue); and (e) the augmented *soc* net.

more easily dispersed homogenously. Similar phenomenon has been reported in our previously work (Wang et al., 2017). As shown in Fig. S8a, H4PPTTA exhibits fluorescent emission at 544 nm upon the excitation at 400 nm, while BUT-22 shows emission at 390 nm upon the excitation at 310 nm. The blue shift of the emission peak of BUT-22 may be attributed to the charge transfer between Al3 + and PPTTA4– ligand. Similar phenomenon has been reported in other literature (Xu and Yan, 2016). On naked eye observation, under excitation at 310 nm using a xenon lamp BUT-22 has a bright blue color, whereas H4PPTTA shows a yellow color when excited with the wavelength of 400 nm (Fig. S8b)." to "The solid-state fluorescent properties of BUT-22 as well as its' ligand acid were firstly measured at RT. As shown in Fig. S8a, H4PPTTA exhibits fluorescent emission at 544 nm upon the excitation at 400 nm, while BUT-22 shows emission at 390 nm upon the excitation at 310 nm. The blue shift of the emission peak of BUT-22 may be attributed to the charge transfer between Al3 + and PPTTA4– ligand. Similar phenomenon has been reported in other literature (Xu and Yan, 2016). On naked eye observation, under excitation at 310 nm using a xenon lamp BUT-22 has a bright blue color, whereas H4PPTTA shows a yellow color when excited with the wavelength of 400 nm (Fig. S8b). For the preparation of the MOF solution for the sensing applications, finely grounded powder samples of BUT-22 were immersed in DMF solution and then ultrasonicated over 30 min to form a steady turbid suspension. Interestingly, we found that the suspension was stable in a short time period of operation. Even after 6 h there is almost no precipitate found in the bottom of the bottle (Fig. S10a). In addition, we also checked the fluorescence of the blank BUT-22 solution at different times. We found that, even after 4 h, the fluorescence of BUT-22 solution was almost the same with the as-prepared one, further confirming the stability of the MOF solution (Fig. S10b). In order to check the consistency of the particle size, SEM of the suspension was measured, and we found the particle size of BUT-22 solution is about 200 nm (Fig. S10c), being basically uniform and quite

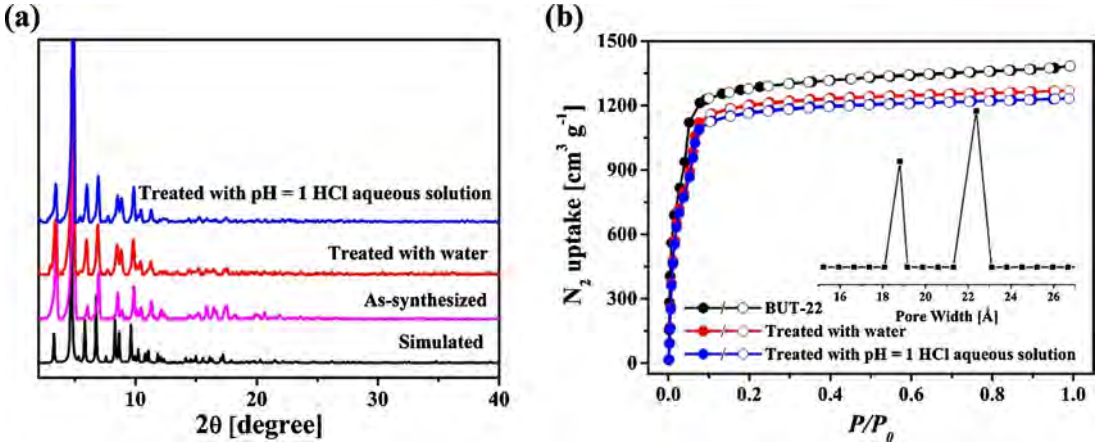

Fig. 2. (a) PXRD patterns of BUT-22 and (b) N_2 adsorption/desorption isotherms at 77 K of BUT-22 samples after treatments in water and pH = 1 HCl aqueous solution for 24 h, respectively (inset shows DFT pore size distribution evaluated by using the N_2 adsorption data).

small. The small and uniform particles are indeed more easily dispersed homogenously. Similar phenomenon has been reported in our previously work (Wang et al., 2017).

Based on its' unique pore structure and good fluorescent property, BUT-22 was explored for the application in the detection of veterinary drugs based on fluorescent sensing. For comparison, the detection ability of Al-soc-MOF-1 toward veterinary drugs was also tested. To explore the ability of BUT-22 and Al-soc-MOF-1 to sense a trace quantity of veterinary drug residues, fluorescence quenching titrations were performed with the piece by piece addition of veterinary drug residues to BUT-22 dispersed in DMF. Six classes of frequently used veterinary drugs: nitrofurans (furazolidone, FZD; nitrofurazone, NZF; nitrofurantoin, NFT), sulfonamides (sulfadiazine, SDZ; sulfamethazine, SMZ sulfamethoxazole, SOM; sulfasalazine, SLA; sulfaclozine, SAZ), tetracyclines (tetracycline, TCY; oxytetracycline, OXY; minocycline, MIN), chloramphenicols (chloramphenicol, CAP), anticoccidial drugs

(dinitolmide, DIN; nicarbazin, NIC) and anthelmintic drugs (niclosamide, NCA) were checked (Fig. S9). For BUT-22, it was found that high fluorescence quenching occurred upon the incremental addition of the veterinary drugs mentioned above (Fig. S11-S25). Fig. 3c shows the percentage of fluorescence quenching in terms of adding a certain amount of different veterinary drugs at RT. It showed that, NZF, NFT, and FZD gave the highest quenching efficiencies of ~98%. In addition, other veterinary drugs present high quenching efficiencies of higher than 82%. For Al-soc-MOF-1, except for DIN, CAP, and SOM, other veterinary drugs gave relative high quenching efficiencies (Fig. S26-S40). Moreover, as shown in Fig. 3c, the quenching efficiencies of BUT-22 are higher than those of Al-soc-MOF-1 for most of the veterinary drugs we studied, except SLA and TCY, indicating its better detection ability.

Interestingly, as shown in Fig. 3a and 3b, when NIC was added, the fluorescence emissions of the two MOFs displayed a significant red shift. Where, 500 μL NIC (0.3 mM) was added the shift wavelength of BUT-22 and Al-soc-MOF-1 is 33 and 29 nm, respectively. Even 20 μL NIC was added, the emissions of the two MOFs display obviously red shift with the changed wavelength of BUT-22 and Al-soc-MOF-1 being 8 and 6 nm, respectively. Other analytes, however, showed no obvious effect on the emission wavelength of the two MOFs (Fig. S11-S40).

The fluorescent quenching efficiency can be quantitatively explained by the Stern-Volmer (SV) equation: $I_0/I = K_{sv}[Q] + 1$, where K_{sv} is the quenching constant (M^{-1}), [Q] is the molar concentration of the analyte, I_0 and I are the luminescence intensities before and after addition of the analyte, respectively (Nagarkar et al., 2013). As indicated in Fig. S11-S40, except for CAP, SDZ, and SMZ, the SV plots for other veterinary drugs are nearly linear at low concentration ranges, but subsequently deviate from linearity and bend upwards at higher concentrations. Such phenomenon of nonlinear SV plots might be due to self-absorption or an energy-transfer process (Shi et al., 2015; Zhang et al., 2014). In Table S2, we list the K_{sv} values of the 15 veterinary drugs, and it was found that the tested veterinary drugs have relatively high K_{sv} values on the two MOFs. Particularly, BUT-22 has the highest K_{sv} value of 209592 M^{-1} toward NZF and Al-soc-MOF-1 has the highest value of 92624 M^{-1} toward SLA. Based on the K_{sv} values and the standard deviations (S_b) from three repeated fluorescent measurements of blank solutions, the limit of detection (LOD, $3S_b/K_{sv}$) of BUT-22 toward these veterinary drugs were calculated (Table S2). BUT-22 has the lowest LOD for NZF (0.07 μM,

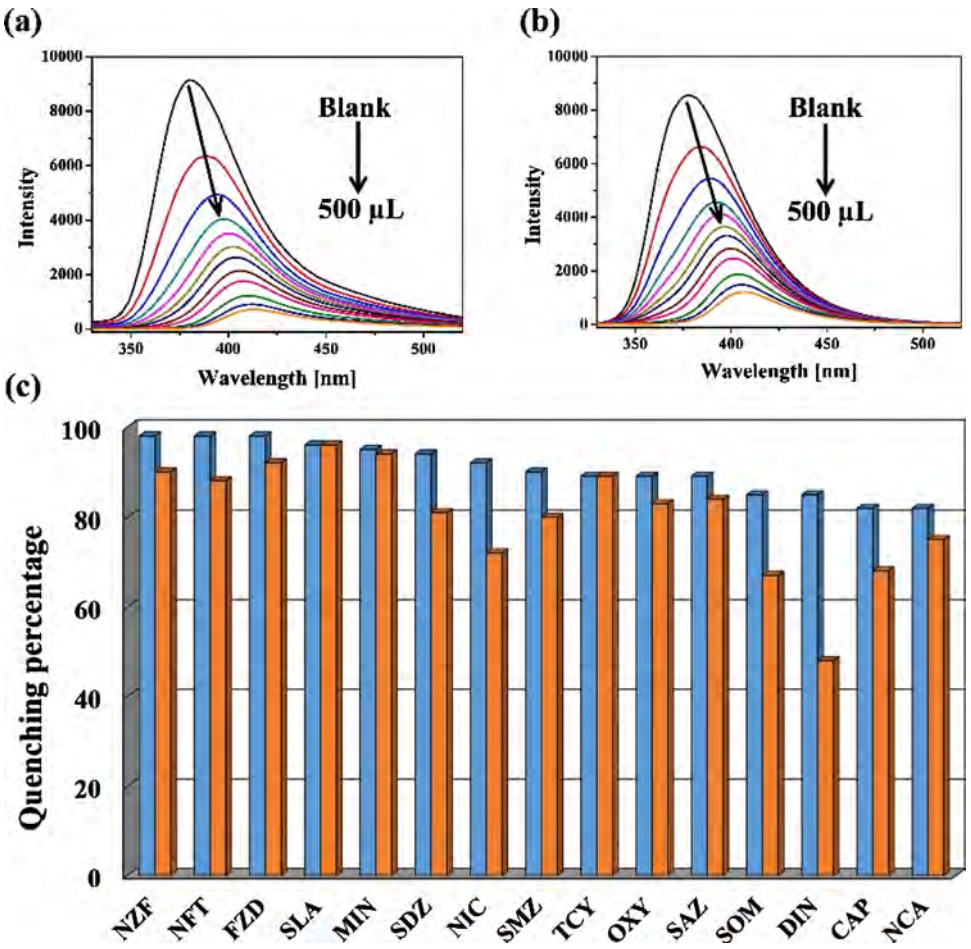

Fig. 3. Effect on the emission spectra of (a) BUT-22 and (b) Al-soc-MOF-1 dispersed in DMF upon incremental addition of NIC (0.3 mM); (c) Fluorescence quenching of BUT-22 (blue bar) and Al-soc-MOF-1 (orange bar) by different veterinary drugs at RT.

corresponding to 14 ppb) and Al-soc-MOF-1 has lowest LOD for SLA (0.09 μM, corresponding to 15 ppb). It should be pointed out that in the previous work we reported the selective detection of NZF by using two Zr-MOFs, BUT-12 and -13. After that, several MOFs such as CTGU-8 (Zhou et al., 2018), $[NaCd_2(L)(BDC)_{2.5}]\cdot 9H_2O$, $[Cd_2(L)(2,6\text{-}NDC)_2]\cdot DMF\cdot 5H_2O$ and $[Cd_2(L)(BPDC)_2]\cdot DMF\cdot 9H_2O$ (Zhao et al., 2017) have also been used for the detection of NZF. The LOD of BUT-12, BUT-13, CTGU-8, $[NaCd_2(L)(BDC)_{2.5}]\cdot 9H_2O$, $[Cd_2(L)(2,6\text{-}NDC)_2]\cdot DMF\cdot 5H_2O$, and $[Cd_2(L)(BPDC)_2]\cdot DMF\cdot 9H_2O$ is 58, 90, 39, 162, 75, and 60 ppb, respectively, all larger than that of BUT-22. A good fluorescent sensor for specific analyte should have low detection limit, the detection ability of BUT-22 toward NZF is thus better than those of all the MOFs mentioned above. In addition, it is interesting to check the sensing ability of BUT-22 toward some real samples and compare the results with those from instrumental analysis. To do this, the waste water from a livestock farm was taken for the test. Firstly, ultra-performance liquid chromatography mass spectrum (UPLC-MS) was used for the analysis of the species and quantity of the veterinary drugs the waste water contains. As shown in Fig. S43, UPLC-MS measurement shows that there exist NFT, NZF, and SDZ in the waste water sample and their concentrations were calculated to be 40.7, 39.6, and 73.2 ppb, respectively. Then, 0.5 mL water sample was added into BUT-22 solution (1.0 mL) to see its' effect on the fluorescence of BUT-22. As shown in Fig. S45, the addition of water sample can slightly quench the fluorescence of BUT-22, and the quenching efficiency is 5%. Obviously, the sensing of veterinary drugs through the fluorescence quenching of BUT-22 is qualitative and cannot district individual species compared with those of conventional ways such as UPLC-MS. However, the operation of our method is easy, and it doesn't need complicated sample pretreatment process which would be more suitable for the rapid and large-scale screening of animal-derived food samples and the self-examination of livestock farms.

Although BUT-22 has excellent detection abilities toward selected 15 veterinary drug molecules, during the screening of commonly used veterinary drugs, however, we found that not all drugs can quench the fluorescence of BUT-22. As shown in Fig. S46a and b, thiamphenicol (THI) and erythrocin (ERY) cannot efficiently quench the fluorescence of BUT-22. The THI slightly enhances the fluorescence of BUT-22 and the quenching efficiency of ERY is only 5% under the same conditions of other selected veterinary drugs. In addition, after checking the structures of the tested veterinary drugs, we found that all nitrofurans molecules contain furan ring and all sulfonamides contain aniline. We thus checked the detection ability of BUT-22 toward furan and aniline. As shown in Fig. S46c and d, the addition of these two molecules can hardly quench the fluorescence of BUT-22. Thus, BUT-22 can selective detect some veterinary drugs, even from other types of substances.

3.4. Detection mechanism analysis

In order to better understand the fluorescence quenching effect of BUT-22 and Al-soc-MOF-1 toward the veterinary drug molecules, the quenching mechanism was proposed. Generally, the quenching on fluorescent MOFs by organic pollutants are mainly explained by the following mechanisms: (1) fluorescence resonance energy transfer (FRET), (2) photoinduced electron transfer (PET), (2) the competition of excitation light between analyte and the MOF, and (4) dynamic/static quenching mechanism (Lustig et al., 2017). FRET occurs only when the emission spectrum of a fluorophore overlaps with the absorption spectrum of the acceptor (Nagarkar et al., 2013). As shown in Fig. 4a, the absorption band of NZF has the greatest degree of overlapping with the emission spectra of BUT-22 and Al-soc-MOF-1, followed by SLA, NFT, FZD, TCY, NIC, MIN, OXY, NCA, SCZ, DIN, and CAP. It should be pointed out that, the absorption band of NZF almost completely overlaps with the emission spectra of two MOFs, thus almost all of the energy of the MOFs emitted through fluorescence transfers to NZF, leading to the complete fluorescence quench of the two MOFs. Indeed, in the detection experiments only 300 μL NZF (0.3 mM) can quench 98% fluorescence of BUT-22. In addition, the absorption bands of SLA, NFT, FZD, TCY, NIC, MIN, OXY, and NCA also overlap the emission spectra of the MOFs well, thus the quenching efficiencies of them are also good. On the contrary, the absorption bands of SDZ, SMZ, and SOM almost have no overlapping with the emission spectra of the two MOFs, but they also have good quenching efficiencies. Thus, FRET is not the only mechanism for the fluorescence quenching observed in these systems.

The PET mechanism is dependent on the energy level of the lowest unoccupied molecular orbital (LUMO) of the MOF and that of the analyte (Nagarkar et al., 2013). If the LUMO energy level of MOF is higher than that of analyte, then the excited electron of the MOF could transfer to the LUMO of the analyte, resulting in the fluorescence quenching. We thus calculated the orbital energies of the LUMOs and highest occupied molecular orbitals (HOMOs) of tested veterinary drugs by density function theory (DFT) calculations (on B3LYP/6-31g*). The HOMO and LUMO energies of the two MOFs were calculated based on cyclic voltammetry (CV) data using a platinum (Pt) disk electrode as the working electrode while Ag/AgCl was used as the reference electrode, similar method has been reported in other works (Fig. S47) (Huang et al. 2013; Zhang et al., 2017b). As shown in Fig. 4b and Table S3, the LUMO energy levels of DIN, NZF, CAP, FZD, and NFT are below those of BUT-22 and Al-soc-MOF-1, while those of other tested analytes are above those of BUT-22 and Al-soc-MOF-1. Thus, in the detection of DIN, NZF, CAP, FZD, and NFT, there exists a PET process. As mentioned above, the absorption spectra of SDZ, SMZ, and SOM have almost no overlap with the emission spectra of the two MOFs, and the LUMO energy levels of them is much higher than those of the two MOFs. Thus, neither FRET nor PET process play a role in the detection of the three veterinary drugs mentioned above.

The competition of the excitation absorption between the analyte and the MOF can also lead to the energy degradation, thereby quenching the fluorescence of the latter (Hu et al., 2015). The work of this mechanism depends on the overlapping between the absorption spectrum of the analyte and the excitation spectrum of the MOF. As shown in Fig. 4c, the absorption spectra of SDZ, SMZ, and SOM almost completely overlap with the emission spectra of the two MOFs. Thus, the three veterinary drugs would compete the energy of excitation light with the two MOFs, leading to the fluorescence quenching of them. In addition, the excitation spectra of the two MOFs also overlap the absorption spectra of other veterinary drugs to some extent, thus the adding of these drug molecules also can quench the fluorescence of the two MOFs.

As discussed above, for most of these checked veterinary drugs, it was found that the quenching efficiencies on BUT-22 are better than those on Al-soc-MOF-1. The only difference of the two MOFs is the existence of pyridine N atoms on the ligand of the former. The pyridine N atoms could collide with the added veterinary drugs, leading to the dynamic quenching. The dynamic quenching process can be confirmed by the changes of the fluorescent lifetimes: if the fluorescent lifetime of veterinary drug incorporated MOF becomes shorter than that of the original MOF, then we can say that the dynamic quenching process occurs (Dong et al., 2015; Xiang et al., 2014). As shown in Fig. 3c, the quenching efficiencies of DIN on the two MOFs have the largest difference, thus we measured the fluorescence lifetimes of the DIN incorporated MOFs and compared them with those of pristine MOFs (Fig. S48). It was found that fluorescent lifetime of BUT-22 shortened from 9.74 to 7.05 ns after the DIN incorporation, thus verifying the existence of the dynamic quenching process. Similarly, after DIN incorporation the fluorescent lifetime of Al-soc-MOF-1 shortened from 7.24 to 6.25 ns, also indicating the existence of dynamic quenching process in it. However, the reduced percentage of the fluorescence lifetime of BUT-22 (28%) is larger than that of Al-soc-MOF-1 (13%) under the same conditions, implying the contribution of the pyridine N atoms in the dynamic quenching process.

In addition, in our previously reported work, we have demonstrated that the pore of MOFs actually plays an important role of the pre-concentrate of analytes, which makes the analytes contact with MOFs more sufficiently, thereby leading to an enhanced florescence response (Wang et al., 2016). Similar phenomenon should happen on BUT-22.

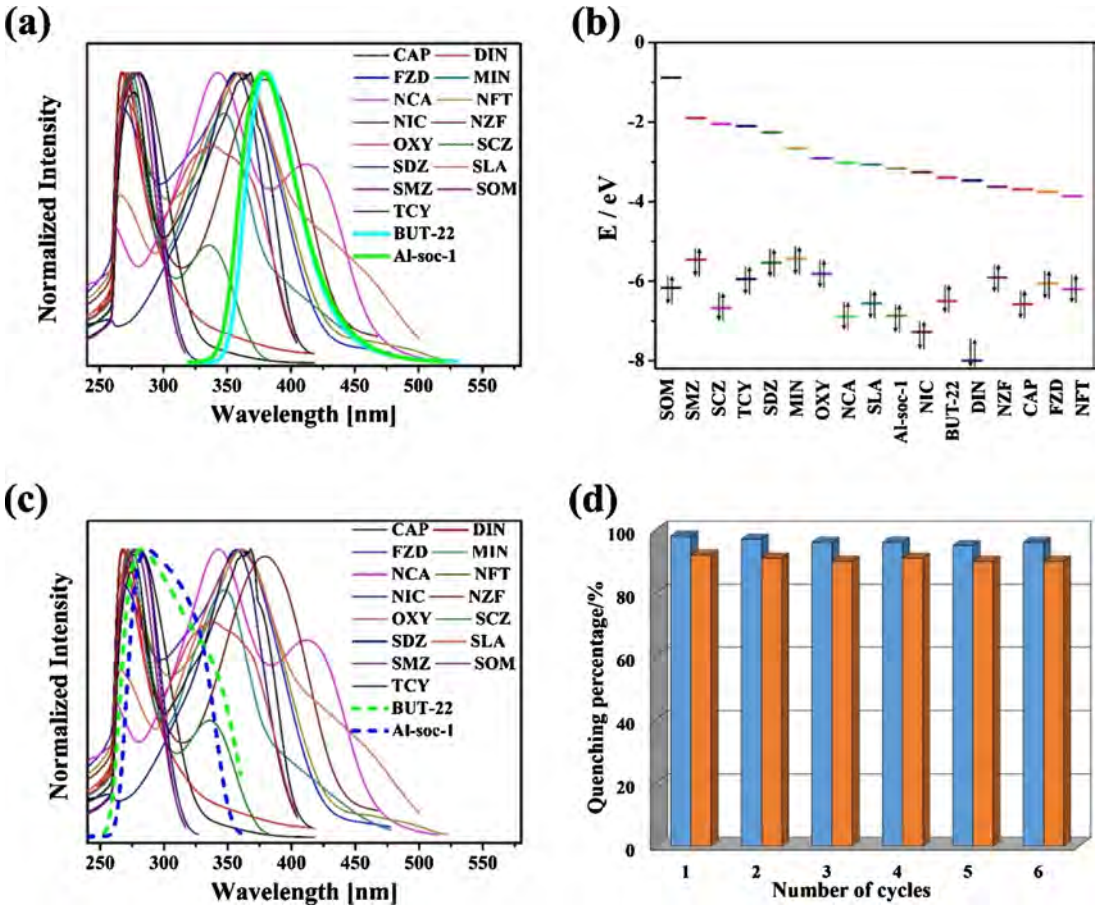

Fig. 4. (a) Overlap between the absorption spectra of veterinary drugs and the emission spectra of BUT-22 and Al-soc-MOF-1 in DMF; (b) HOMO and LUMO energies for tested veterinary drugs and MOFs arranged in descending order of LUMO energies; (c) overlap between the absorption spectra of veterinary drugs and the excitation spectra of BUT-22 and Al-soc-MOF-1 in DMF; and (d) reproducibility of the quenching ability of BUT-22 (blue bar) and Al-soc-MOF-1 (orange bar) by NZF.

Besides, the sensing is mainly occurred in the pores of MOFs. To confirm this hypothesis, the adsorption experiments of BUT-22 toward three representative veterinary drugs with different sizes, NZF, TCY, and ERY (the size of which is 8.9 × 4.1, 14.1 × 6.9, and 14.1 × 13.4 Å, respectively, Fig. S49a-c) were performed. It should be pointed out that the size of ERY is almost the same as the channel size of BUT-22 (15 Å) when van der waals radius was considered. Experimentally, freshly prepared BUT-22 sample (10 mg) was totally activated and then transferred into DMF solution of NZF (or TCY and ERY) with given concentration and volume (10 ppm, 5 mL) in a vial, respectively. UV–vis spectra of the solutions were recorded in-suit to characterize the adsorption performance of BUT-22 along with the soaking time at 298 K. As shown in Fig. S49d and e, BUT-22 represents high adsorption rates toward NZF and TCY and the removal efficiencies BUT-22 toward NZF and TCY are 72 and 51%, respectively. The intensity of ERY, however, almost has no change even after adsorption for 270 min, which means that BUT-22 cannot absorb ERY in its pores (Fig. S49f). As mentioned above, the addition of ERY (500 μL) can only quench the fluorescence of BUT-22 in 5%, which is largely different from NZF and TCY (quenching efficiencies of 98 and 90%, respectively). As mentioned above, the adsorption ability of BUT-22 toward NZF is better than that of TCY and the calculated detection limit of BUT-22 toward the former is lower than the latter. These results clearly show that the sensing is mainly occurred in the pores of MOFs, those molecules with larger size cannot contact efficiently with the pore walls of MOF, thus leading to relative low fluorescence quenching. To further confirm the enrichment of veterinary drug molecules can enhance the sensitivity of fluorescence response, fluorescent titration experiments were carried out on the only H_4PPTTA ligand toward NZF and TCY. Using the same conditions as the MOF, we observed that NZF can quench the fluorescence of H_4PPTTA in 57%, but TCY can hardly affect the fluorescence of H_4PPTTA (Fig. S50). Although the emission of free ligand could still be quenched by the NZF, however, the calculated K_{sv} is 12820 M^{-1}, far smaller than that of BUT-22 under the same conditions (70949 M^{-1}). This comparison clearly proves the sensitization effect of MOF adsorption on the fluorescent sensing of veterinary drugs. Overall, based on multiple mechanisms including FRET, PET, competition of the excitation absorption, dynamic quenching, and pre-concentrate of analytes in the pores, the two MOFs, especially BUT-22, exhibit excellent detection abilities toward the 15 normally used veterinary drugs.

In addition, as mentioned above the addition of NIC into the MOF DMF solutions can make the fluorescence emission spectra of them shift to higher wavelength. This unique property allows us to easily distinguish NIC from other veterinary drugs. Actually, NIC is a mixture of 4,4′-dinitros-diphenylurea (DNC) and 2-hydroxy-4,6-dimethylpyrimidine (HDP) in equal molecular proportions. In order to further clarify which molecule played the key role in inducing the shift of the fluorescent emissions of MOFs, we tested the influences of them on the MOF fluorescence separately. As shown in Fig. S41 and S42, adding HDP can only quench the fluorescence of the two MOFs, but DNC can both quench and shift the fluorescence emissions of the two MOFs to higher wavelength. As shown in Fig. S9, the structure of DNC is highly coplanar. Therefore, we propose that the red shift of the fluorescence emissions of the MOFs is probably due to the presence of weak interactions such as π-π stacking or hydrogen bonding interactions between the DNC molecules and the skeleton of the MOFs. These weak interactions will change the electronic structures of MOFs, further change the fluorescence emission of them. Similar phenomenon has been

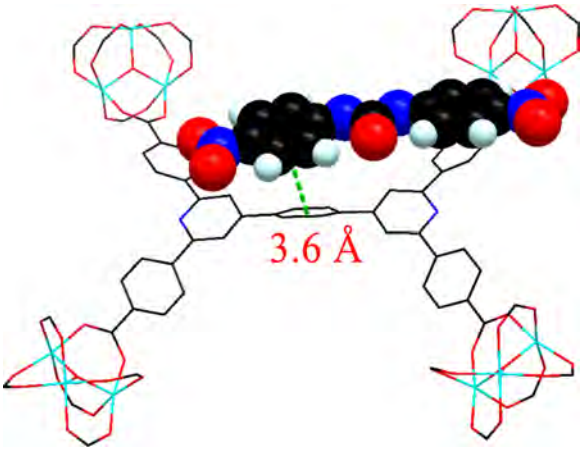

Fig. 5. Optimized geometry for identifying the interaction of DNC with BUT-22 (color code: Al, wathet-blue; C, black; O, red; and N, blue).

reported in the selective detection of NH_3 by using Zn_2(TCPE) and Mg (H_2DHBDC) (Shustova et al., 2013). In addition, the π-π stacking induced red shifting of fluorescence emission wavelength has also been reported in the mechanofluorochromic carbon nanodots (Liu et al., 2018) and organic molecular (Dong et al., 2012). To confirm the presence of the weak interactions between DNC and MOFs, we carried out a structural optimization on the DNC-loaded BUT-22 by using the Materials Studio Sorption Package (on the grand canonical monte carlo (GCMC) method and Burchard universal force field) (Lin et al., 2018). As shown in Fig. 5, the loaded DNC molecule was found to be parallel to the ligand in BUT-22, and the distance between one benzene ring of DNC and the central benzene ring of $PPTTA^{4-}$ ligand is about 3.6 Å, verifying the existence of strong π-π stacking interaction between them.

3.5. Cyclic use test

As molecule sensor, the cyclic use is an important issue. Thus, we also studied the regeneration of the two MOFs after used in sensing the veterinary drugs. The detailed process is shown in the Experimental Section. It was found that the quenching efficiencies of the two MOFs toward NZF are basically unchanged up to six cycles, demonstrating their good recyclability and stability for the detection application (Fig. 4d).

4. Conclusions

A new highly stable fluorescent Al(III)-based MOF with a *soc*-a topological framework structure, BUT-22 has been designed and synthesized. This MOF has a similar structure with reported Al-soc-MOF-1 but difference in the pyridine N functionalized ligand used. The two MOFs have moderate pore size and represent excellent detection ability with good recyclability and stability towards 15 normally used veterinary drugs in terms of distinct fluorescent quenching. The quenching efficiencies are all beyond 82%, and the BUT-22 also represents very low limit of detection. Particularly, the limit of detection of BUT-22 toward NZF is 14 ppb. In addition, the two MOFs can also selectively detect NIC based on the observed red shift of their emission spectra. A synergetic effect from multiple mechanisms is believed to be the main reasons for the observed excellent detection ability. The two MOFs are therefore potentially useful in the broad spectrum detection of veterinary drugs. Clearly, MOFs as a kind of new platform have great application potential in the food safety field, and expanding exploration is going on in our lab.

Declaration of Competing Interest

The authors declare no competing financial interest.

Acknowledgements

We acknowledge financial support from the National Natural Science Foundation of China (No. 21576006, 51621003, 21771012) and National Key Research and Development Program of China (No. 2018YFC1902506).

Appendix A. Supplementary data

Supplementary material related to this article can be found, in the online version, at doi:https://doi.org/10.1016/j.jhazmat.2019.121018.

References

Ritter, L., Goushleff, N.C., Arbuckle, T., Cole, D., Raizenne, M., 2006. Addressing the linkage between exposure to pesticides and human health effects-research trends and priorities for research. J. Toxicol. Eenviron. Heal. B 9, 441–456.
Passantino, A., Russo, C., 2008. Maximum residue levels of veterinary medicines in relation to food safety: european community legislation and ethical aspects. J. Verbrauch. Lebensm. 3, 351–358.
Iglesias-Garcia, I., Barriada-Pereira, M., Gonzalez-Castro, M.J., Muniategui-Lorenzo, S., Lopez-Mahia, P., Prada-Rodriguez, D., 2008. Development of an analytical method based on microwave-assisted extraction and solid phase extraction cleanup for the determination of organochlorine pesticides in animal feed. Anal. Bioanal. Chem. 391, 745–752.
Aulakh, R.S., Gill, J.P.S., Bedi, J.S., Sharma, J.K., Joia, B.S., Ockerman, H.W., 2006. Organochlorine pesticide residues in poultry feed, chicken muscle and eggs at a poultry farm in Punjab, India. J. Environ. Sci. Health B 86, 741–744.
Fernandez-Alvarez, M., Llompart, M., Lamas, J.P., Lores, M., Garcia-Jares, C., Garcia-Chao, M., Dagnac, T., 2009. Simultaneous extraction and cleanup method based on pressurized solvent extraction for multiresidue analysis of pesticides in complex feed samples. J. Agric. Food Chem. 57, 3963–3973.
Guo, Y., Yu, H.Y., Zhang, B.Z., Zeng, E.Y., 2009. Persistent halogenated hydrocarbons in fish feeds manufactured in South China. J. Agric. Food Chem. 57, 3674–3680.
Carro, A.M., Lorenzo, R.A., Ferńandez, R.R.F., Cela, R., 2005. Multi-residue screening of chlorinated and brominated compounds from aquaculture samples using matrix solid-phase dispersion-gas chromatography-mass spectrometry. J. Chromatogr. A 1071, 93–98.
You, L., Zha, D., Anslyn, E.V., 2015. Recent advances in supramolecular analytical chemistry using optical sensing. Chem. Rev. 115, 7840–7892.
Kreno, L.E., Leong, K., Farha, O.K., Allendorf, M., Van Duyne, R.P., Hupp, J.T., 2012. Metal-organic framework materials as chemical sensors. Chem. Rev. 112, 1105–1125.
Lustig, W.P., Mukherjee, S., Rudd, N.D., Desai, A.V., Li, J., Ghosh, S.K., 2017. Metal-organic frameworks: functional luminescent and photonic materials for sensing applications. Chem. Soc. Rev. 46, 3242–3285.
Wang, X.S., Li, L., Yuan, D.Q., Huang, Y.B., Cao, R., 2018. Fast, highly selective and sensitive anionic metal-organic framework with nitrogen-rich sites fluorescent chemosensor for nitro explosives detection. J. Hazard. Mater. 344, 283–290.
Zhu, X.D., Zhang, K., Wang, Y., Long, W.W., Sa, R.J., Liu, T.F., Lu, J., 2018. Fluorescent metal-organic framework (MOF) as a highly sensitive and quickly responsive chemical sensor for the detection of antibiotics in simulated wastewater. Inorg. Chem. 57, 1060–1065.
Sawano, T., Thacker, N.C., Lin, Z., McIsaac, A.R., Lin, W., 2015. Robust, chiral, and porous BINAP-based metal-organic frameworks for highly enantioselective cyclization reactions. J. Am. Chem. Soc. 137, 12241–12248.
Zhang, S.Y., Wojtas, L., Zaworotko, M.J., 2015. Structural insight into guest binding sites in a porous homochiral metal-organic material. J. Am. Chem. Soc. 137, 12045–12049.
Li, B., Wen, H.M., Wang, H., Wu, H., Tyagi, M., Yildirim, T., Zhou, W., Chen, B., 2014. A porous metal-organic framework with dynamic pyrimidine groups exhibiting record high methane storage working capacity. J. Am. Chem. Soc. 136, 6207–6210.
Spanopoulos, I., Tsangarakis, C., Klontzas, E., Tylianakis, E., Froudakis, G., Adil, K., Belmabkhout, Y., Eddaoudi, M., Trikalitis, P.N., 2016. Reticular synthesis of HKUST-like tbo-MOFs with enhanced CH_4 storage. J. Am. Chem. Soc. 138, 1568–1574.
Nugent, P., Belmabkhout, Y., Burd, S.D., Cairns, A.J., Luebke, R., Forrest, K., Pham, T., Ma, S., Space, B., Wojtas, L., Eddaoudi, M., Zaworotko, M.J., 2013. Porous materials with optimal adsorption thermodynamics and kinetics for CO_2 separation. Nature 495, 80–84.
Cui, X., Chen, K., Xing, H., Yang, Q., Krishna, R., Bao, Z., Wu, H., Zhou, W., Dong, X., Han, Y., Li, B., Ren, Q., Zaworotko, M.J., Chen, B., 2016. Pore chemistry and size control in hybrid porous materials for acetylene capture from ethylene. Science 353, 141–144.
Liao, P.Q., Huang, N.Y., Zhang, W.X., Zhang, J.P., Chen, X.M., 2017. Controlling guest conformation for efficient purification of butadiene. Science 356, 1193–1196.
Hu, Z., Wang, Y., Shah, B.B., Zhao, D., 2018. CO_2Capture in Metal-Organic Framework Adsorbents: An Engineering Perspective. Adv. Sustainable Syst. 3, 1800080.
Jiang, J., Gandara, F., Zhang, Y.-B., Na, K., Yaghi, O.M., Klemperer, W.G., 2014. Superacidity in sulfated metal-organic framework-808. J. Am. Chem. Soc. 136, 12844–12847.
Yang, X., Sun, J.-K., Kitta, M., Pang, H., Xu, Q., 2018. Encapsulating highly catalytically active metal nanoclusters inside porous organic cages. Nat. Catal. 1, 214–220.
Zhang, X., Huang, Z., Ferrandon, M., Yang, D., Robison, L., Li, P., Wang, T.C., Delferro,

M., Farha, O.K., 2018. Catalytic chemoselective functionalization of methane in a metal – organic framework. Nat. Catal. 1, 356–362.
Tang, J., Wang, J., 2018. Metal organic framework with coordinatively unsaturated sites as efficient fenton-like catalyst for enhanced degradation of sulfamethazine. Environ. Sci. Technol. 52, 5367–5377.
Zhang, F., Zhao, C., Chen, S., Li, H., Yang, H., Zhang, X.-M., 2017a. In situ mosaic strategy generated Co-based N-doped mesoporous carbon for highly selective hydrogenation of nitroaromatics. J. Catal. 348, 212–222.
Deria, P., Gomez-Gualdron, D.A., Hod, I., Snurr, R.Q., Hupp, J.T., Farha, O.K., 2016. Framework-topology-Dependent catalytic activity of zirconium-based (Porphinato) zinc(II) MOFs. J. Am. Chem. Soc. 138, 14449–14457.
Joarder, B., Lin, J.B., Romero, Z., Shimizu, G.K.H., 2017. Single crystal proton conduction study of a metal organic framework of modest water stability. J. Am. Chem. Soc. 139, 7176–7179.
Liu, W., Dai, X., Bai, Z., Wang, Y., Yang, Z., Zhang, L., Xu, L., Chen, L., Li, Y., Gui, D., Diwu, J., Wang, J., Zhou, R., Chai, Z., Wang, S., 2017. Highly sensitive and selective uranium detection in natural water systems using a luminescent mesoporous metal-organic framework equipped with abundant lewis basic sites: a combined batch, X-ray absorption spectroscopy, and first principles simulation investigation. Environ. Sci. Technol. 51, 3911–3921.
N'Dala-Louika, I., Ananias, D., Latouche, C., Dessapt, R., Carlos, L.D., Serier-Brault, H., 2017. Ratiometric mixed Eu–Tb metal–organic framework as a new cryogenic luminescent thermometer. J. Mater. Chem. C 5, 10933–10937.
Wang, B., Lv, X.L., Feng, D.W., Xie, L.H., Zhang, J., Li, M., Xie, Y.B., Li, J.R., Zhou, H.C., 2016. Highly stable Zr(IV)-based metal-organic frameworks for the detection and removal of antibiotics and organic explosives in water. J. Am. Chem. Soc. 138, 6204–6216.
Bai, Y., Dou, Y., Xie, L.-H., Rutledge, W., Li, J.-R., Zhou, H.-C., 2016. Zr-based metal-organic frameworks: design, synthesis, structure, and applications. Chem. Soc. Rev. 45, 2327–2367.
Yang, C.X., Ren, H.B., Yan, X.P., 2013. Fluorescent metal organic framework MIL-53(Al) for highly selective and sensitive detection of Fe^{3+} in aqueous solution. Anal. Chem. 85, 7441–7446.
Wang, B., Yang, Q., Guo, C., Sun, Y., Xie, L.-H., Li, J.-R., 2017. Stable Zr(IV)-based metal-organic frameworks with predesigned functionalized ligands for highly selective detection of Fe(III) ions in water. ACS Appl. Mater. Inter. 9, 10286–10295.
Alezi, D., Belmabkhout, Y., Suyetin, M., Bhatt, P.M., Weselinski, L.J., Solovyeva, V., Adil, K., Spanopoulos, I., Trikalitis, P.N., Emwas, A.-H., Eddaoudi, M., 2015. MOF crystal chemistry paving the way to gas storage needs: Aluminum-based soc-MOF for CH_4, O_2, and CO_2 Storage. J. Am. Chem. Soc. 137, 13308–13318.
Spek, A.L., 2003. Single-crystal structure validation with the program PLATON. J. Appl. Crystallogr. 36, 7–13.
Rappe, A.K., Colwell, K.S., Casewit, C.J., 1993. Application of a universal force field to metal complexes. Inorg. Chem. 32, 3438–3450.
Xu, X.Y., Yan, B., 2016. An efficient and sensitive fluorescent pH sensor based on amino functional metal-organic frameworks in aqueous environment. Dalton Trans. 45, 7078–7084.
Nagarkar, S.S., Joarder, B., Chaudhari, A.K., Mukherjee, S., Ghosh, S.K., 2013. Highly selective detection of nitro explosives by a luminescent metal-organic framework. Angew. Chem. Int. Ed. 52, 2881–2885.
Shi, Z.Q., Guo, Z.J., Zheng, H.G., 2015. Two luminescent Zn(II) metal-organic frameworks for exceptionally selective detection of picric acid explosives. Chem. Commun. 51, 8300–8303.
Zhang, Q., Geng, A., Zhang, H., Hu, F., Lu, Z.H., Sun, D., Wei, X., Ma, C., 2014. An independent 1D single-walled metal-organic nanotube transformed from a 2D layer exhibits highly selective and reversible sensing of nitroaromatic compounds. Chem. Eur. J. 20, 4885–4890.
Zhou, Z.H., Dong, W.W., Wu, Y.P., Zhao, J., Li, D.S., Wu, T., Bu, X.H., 2018. Ligand-controlled integration of Zn and Tb by photoactive terpyridyl-functionalized tricarboxylates as highly selective and sensitive sensors for nitrofurans. Inorg. Chem. 57, 3833–3839.
Zhao, D., Liu, X.-H., Zhao, Y., Wang, P., Liu, Y., Azam, M., Al-Resayes, S.I., Lu, Y., Sun, W.-Y., 2017. Luminescent Cd(II)–organic frameworks with chelating NH_2 sites for selective detection of Fe(III) and antibiotics. J. Mater. Chem. A Mater. Energy Sustain. 5, 15797–15807.
Huang, J., Sun, N., Dong, Y., Tang, R., Lu, P., Cai, P., Li, Q., Ma, D., Qin, J., Li, Z., 2013. Similar or totally different: the control of conjugation degree through minor structural modifications, and deep-blue aggregation-induced emission luminogens for non-doped OLEDs. Adv. Funct. Mater. 23, 2329–2337.
Zhang, D., Qiao, J., Zhang, D., Duan, L., 2017b. Ultrahigh-efficiency gGreen PHOLEDs with a voltage under 3 V and a power efficiency of nearly 110 lm W^{-1} at luminance of 10 000 cd m^{-2}. Adv. Mater. 29, 1702847.
Hu, Z., Lustig, W.P., Zhang, J., Zheng, C., Wang, H., Teat, S.J., Gong, Q., Rudd, N.D., Li, J., 2015. Effective detection of mycotoxins by a highly luminescent metal-organic framework. J. Am. Chem. Soc. 137, 16209–16215.
Dong, X.Y., Wang, R., Wang, J.Z., Zang, S.Q., Mak, T.C.W., 2015. Highly selective Fe^{3+} sensing and proton conduction in a water-stable sulfonate-carboxylate Tb-organic-framework. J. Mater. Chem. A 3, 641–647.
Xiang, Z.H., Fang, C.Q., Leng, S.H., Cao, D.P., 2014. An amino group functionalized metal-organic framework as a luminescent probe for highly selective sensing of Fe^{3+} ions. J. Mater. Chem. A 2, 7662–7665.
Shustova, N.B., Cozzolino, A.F., Reineke, S., Baldo, M., Dinca, M., 2013. Selective turn-on ammonia sensing enabled by high-temperature fluorescence in metal-organic frameworks with open metal sites. J. Am. Chem. Soc. 135, 13326–13329.
Liu, C., Xiao, G., Yang, M., Zou, B., Zhang, Z.L., Pang, D.W., 2018. Mechanofluorochromic carbon nanodots: controllable pressure-triggered blue- and red-shifted photoluminescence. Angew. Chem. Int. Ed. 57, 1893–1897.
Dong, Y., Xu, B., Zhang, J., Tan, X., Wang, L., Chen, J., Lv, H., Wen, S., Li, B., Ye, L., Zou, B., Tian, W., 2012. Piezochromic luminescence based on the molecular aggregation of 9,10-bis((E)-2-(pyrid-2-yl)vinyl)anthracene. Angew. Chem. Int. Ed. 51, 10782–10785.
Lin, S., Zhao, Y., Yun, Y.S., 2018. Highly effective removal of nonsteroidal anti-inflammatory pharmaceuticals from water by Zr(IV)-Based metal-organic framework: adsorption performance and mechanisms. ACS Appl. Mater. Inter. 10, 28076–28085.